SCIENCE CHINA Materials ARTICLES

mater.scichina.com link.springer.com

Published online 22 July 2020 | https://doi.org/10.1007/s40843-020-1372-6
Sci China Mater 2021, 64(1): 169–178

Polymorph and anisotropic Raman spectroscopy of Phz-H_2ca cocrystals

Weigang Zhu[1,2], Yunli Wang[3], Chengcheng Huang[4], Lingyun Zhu[5], Yonggang Zhen[1], Huanli Dong[1], Zhixiang Wei[5], Dong Guo[3,4] and Wenping Hu[1,6*]

ABSTRACT **The nucleation and growth mechanism and polymorph-property correlations in the molecular cocrystal field are widely sought but currently remain unclear. Herein, a new wire-like morphology of phenazine (Phz)-chloranilic acid (H_2ca) cocrystal (PHC) is demonstrated for the first time, and the self-assembly of Phz and H_2ca is controlled to selectively prepare kinetically stable wires and thermodynamically stable plates. Specifically, low precursor concentration is beneficial for one-dimensional (1D) self-assembly along the [010] crystallographic direction, while only supersaturation can trigger 2D self-assembly along the [100] and [010] directions, respectively. This is understandable in terms of the (020) face showing the largest attachment energy (E_{att}) and the (002) face possessing the smallest surface energy (E_{surf}). Moreover, anisotropic Raman spectra related to the mode symmetry and atomic displacements in two types of PHCs are revealed, and the same Raman-active vibrational bands of PHC wire and plate show different polarization responses, which is intrinsically ascribed to their different molecular orientations. Overall, this is the first case that morphologies of cocrystal are precisely tuned with comprehensive investigations of their anisotropic vibrational characteristics.**

Keywords: molecular cocrystal, polymorph, self-assembly, Raman spectroscopy, anisotropy

INTRODUCTION

Single crystals of organic molecule [1] and polymer [2,3] with few grain boundaries, defects, traps and impurities, are ideal for fundamental research and advanced applications in electronics [4,5], photonics [6,7], spintronics [8,9], and energy science and technology [10,11]. Molecular cocrystal (also named as "co-crystal"), similarly, a highly single-crystalline single phase material composed of two, three or more different compounds in a specific stoichiometric ratio [12], shows new, unpredicted physicochemical properties based on the multi-component synergistic and collective (MCSC) effect [13]. Examples include white-light emitting [14], ambipolar charge carrier transport [15], ferroelectricity [16,17], room-temperature phosphorescence (RTP) [18], and optical second harmonic generation (SHG) [19,20]. In contrast to crystals of singe-component material, co-crystallization offers an alternative but efficient approach for achieving multifunctional smart materials, and a material research paradise for exploring new chemical and physical phenomena, properties, and functionalities [13,21]. For the property-oriented materials science research, co-crystallization is easier, greener and more efficient than the conventional organic synthesis. However, one of the best-known challenges in this research field is effective co-crystallization between different molecules towards desired functions [22], while the nucleation and growth mechanism of molecular cocrystal is key but remains largely elusive [23], which in fact prevents further rational design and synthesis of functional cocrystals, arrays, and devices [10].

Our laboratory is interested in such fundamental questions and has been directing this research field since 2012 [24,25]. Fortunately, polymorph of cocrystals offers

[1] Laboratory of Organic Solids, Institute of Chemistry, Chinese Academy of Sciences, Beijing 100190, China
[2] University of Chinese Academy of Sciences, Beijing 100049, China
[3] Institute of Acoustics, Chinese Academy of Sciences, Beijing 100190, China
[4] School of Materials Science and Engineering, Beihang University, Beijing 100191, China
[5] National Center for Nanoscience and Technology, Beijing 100190, China
[6] Tianjin Key Laboratory of Molecular Optoelectronic Sciences, Department of Chemistry, School of Science, Tianjin University & Collaborative Innovation Center of Chemical Science and Engineering (Tianjin), Tianjin 300072, China
* Corresponding author (email: huwp@tju.edu.cn)

the possibility to answer these fundamental questions, due to their distinct different molecular packings, self-assembling manners and the resulting crystal morphologies [10]. In this regard, governing the molecular self-assembly and crystal growth kinetics of these micro-nano cocrystal systems to obtain individual ones with definite crystal phase, morphology and size becomes particularly important, because it in turn helps to understand the intrinsic cocrystal formation and growth mechanism, establish the structure-function relationships [10], and is convenient for large-area device fabrications and applications [26,27]. However, selective synthesis of cocrystals is challenging, because (i) similar to single-component-material crystals [28], different polymorphs of cocrystal always crystallize concomitantly in one-pot process [29–31]; (ii) the theoretical models for single crystal growth, such as the Kossel-Stranski model and Bravais rule [24], might be not suitable for molecular cocrystals; (iii) some cocrystals with segregated-stacking are not stable [32], and phase transition is easy to happen at ambient conditions [33,34].

With these considerations in mind, we herein choose phenazine (**Phz**) and chloranilic acid (**H_2ca**, Fig. 1a) as the prototype, which previously form hydrogen-bonded (H-bond) cocrystals with plate-like morphology by slow evaporation of mixed solution (Fig. S1) or by the co-sublimation in a vacuum-sealed glass tube [16]. We demonstrate, for the first time, that a new wire-like morphology is selectively obtained and fully experimentally confirmed by atomic force microscopy (AFM), transmission electron microscopy (TEM), X-ray diffraction (XRD), ultraviolet-visible (UV-Vis) absorption spectroscopy, differential scanning calorimetry (DSC), and solid-state nuclear magnetic resonance (NMR) measurements. The solution self-assembly of **Phz** and **H_2ca** is controlled by tuning the precursor concentration in solvent evaporation to form kinetically stable **Phz-H_2ca** cocrystal (PHC) wires and thermodynamically stable PHC plates, which is attributed to the Material Studio software simulation results that the (020) face of PHC shows the largest attachment energy (E_{att}) and the (002) face possesses the smallest surface energy (E_{surf}). This thereby allows us to propose a nucleation and growth mechanism for PHC, providing a standard reference for further controlling polymorph of organic cocrystals. Moreover, different polarizations of Raman characteristic peaks in the anisotropic experiments related to the mode symmetry and atomic displacements of PHC wire (or plate)

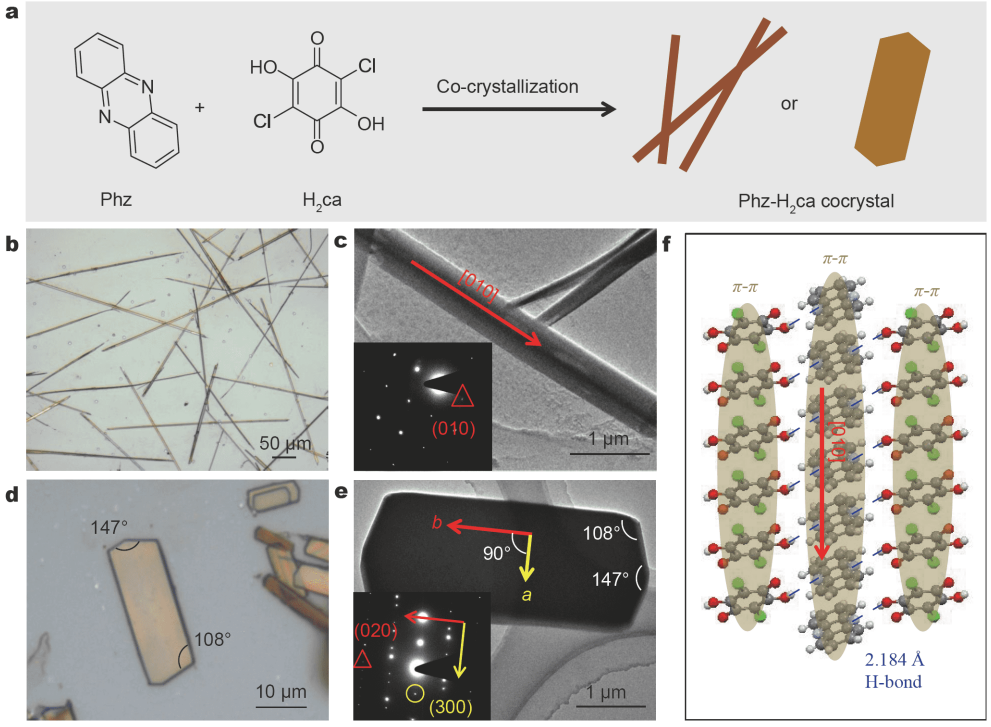

Figure 1 Cocrystal morphology and structure. (a) Co-crystallization of **Phz** and **H_2ca** toward wire- and plate-like **Phz-H_2ca** crystals. The optical images of (b) wires and (d) plates on glass substrate. TEM and SAED images of individual (c) wire and (e) plate. (f) The corresponding molecular packing and intermolecular interactions in PHC.

are revealed. It will be seen that the same Raman bands of two types of PHCs exhibit different anisotropic responses, which are intrinsically attributed to their different molecular orientations. The results herein help to rationally control the polymorph of cocrystals, and gain a deeper understanding of intrinsic physicochemical properties in molecular solids.

EXPERIMENTAL SECTION

Materials, chemicals, and all the experimental details can be found in the Supplementary information.

RESULTS AND DISCUSSION

Structures and characterizations of wires

The **Phz** and **H_2ca** molecules self-assemble into wire- (Fig. 1b) and plate-like (Fig. 1d, and Fig. S2) crystals, which are clearly different from those of single-component-material crystals (Figs S3–S5), and the intersection angles of hexagon plate are found to be 147° and 108°, respectively. The XRD patterns of these wires and plates on glass substrates are different from those of **Phz** and **H_2ca** crystals (Figs S6–S10) but in accord with the simulated pattern exported from the .cif file of PHC (room-temperature phase, CCDC 269940, Tables S1, S2, and Fig. S11) [35]. It indicates that the wires and plates are in fact the cocrystals of **Phz** and **H_2ca**, and both of them belong to the same cocrystal phase (Fig. S12). Note that the plate-like morphology of PHC has been demonstrated in 2005 [16], while the wire-like morphology has not yet.

To further confirm the cocrystal nature of the obtained wires, they were collected under low solution concentration. The obtained crystal powder shows black color (Fig. 2a), which is clearly different from **Phz** (light-yellow) and **H_2ca** (red) crystals. The corresponding absorption spectra (Fig. 2b) are consistent with the cocrystal color, and show significantly red-shifted absorption, which is not simply the sum of those collected from individual component crystals. Similarly, the DSC measurement of the wires (Fig. S13) shows only one strong melting peak (272.4°C) [36], which is lower than **H_2ca** crystals (282°C)[37], but higher than **Phz** crystals (176°C) [38], reflecting a new single-phase solid with different intermolecular interactions from **Phz** or **H_2ca**. Moreover, the chemical shift (~10 ppm) of **H_2ca** is changed to 13.5 ppm in the ^{1}H NMR spectra of wires (Fig. 2c and Fig. S15), demonstrating the formation of H-bond. Overall, these allow us to conclude that the obtained wire is a new morphology of **Phz-H_2ca** cocrystal.

The TEM and selected area electron diffraction (SAED) images of PHC wire and plate (Fig. 1c, e) indicate they are highly single crystalline. The crystal structure of PHC belongs to the space group of $P2_1/n$ with cell parameters of a=12.399 Å, b=3.853 Å, c=16.957 Å, α=90°, β=107.89°, γ=90° [35], and thus the SAED pattern collected from individual wire with d-spacing value of 3.92 Å can be

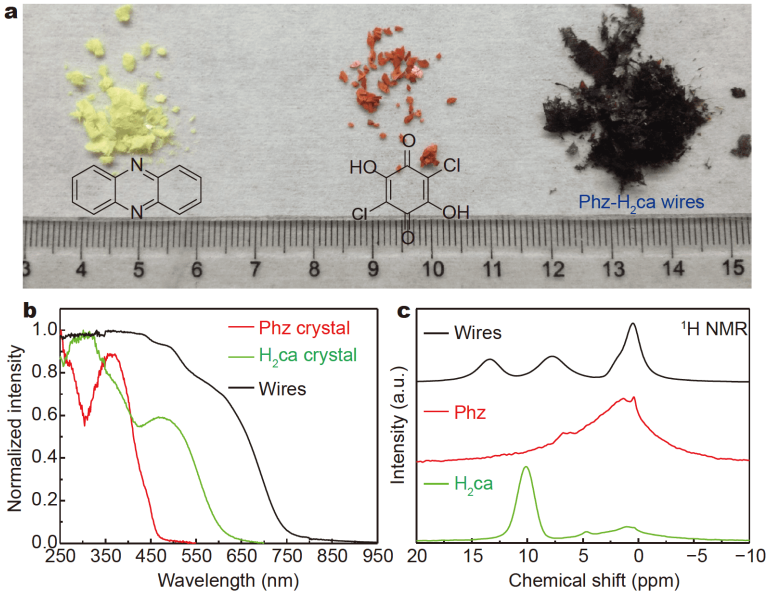

Figure 2 Characterizations of PHC wires. (a) The optical images of **Phz**, **H_2ca** crystals, and PHC wires. (b) The typical absorption spectra of **Phz**, **H_2ca** crystals, and PHC wires on quartz slides The absorption spectrum fitting result of PHC wires is shown in Fig. S14. (c) The solid-state ^{1}H NMR result. More detailed results can be found in Fig. S15.

indexed to (010), showing that it grows along the [010] direction. This is also verified by the XRD result (Fig. S6), in which *b* miller index is not observed. In contrast, only (002) peak appears in the XRD pattern of plates, and the *d*-spacing values with intersection angle 90° of individual plate are attributed to (100) and (010), respectively, which illustrates the hexagon plate grows along the [100] and [010] directions. In order to reveal the driving forces for the PHCs' growth, Fig. 1f shows that molecules pack in a segregated fashion with π-π interactions in both of the **Phz** and **H_2ca** molecular columns (Fig. S11), which are connected with each other by strong hydrogen bonds (2.184 Å), resulting in a unique supramolecular architecture. In this sense, the π-π interactions are the driving force for the 1D growth of wires, and also responsible for [010] growth of plates with another direction ([100]) contributed from the hydrogen bonds.

Cocrystal nucleation and growth

The self-assembly of **Phz** and **H_2ca** is controlled by changing the applied experimental conditions to prepare PHC wires and plates. In a typical experiment, PHCs were obtained by using a solution drop-casting method (Fig. S1). **Phz** and **H_2ca** show good solubility in acetonitrile solvent (Fig. 3a), but when the two materials were mixed (1.8 mg **Phz** + 2.1 mg **H_2ca** + 5 mL CH_3CN in the vial), the solution surprisingly became muddy. From drop-casting of the muddy suspension immediately, we obtained both of wires and plates on the substrate (Fig. 3b) but no spare **Phz** and **H_2ca** crystals were determined (see the XRD in Fig. S8). The similar case was also observed, even if less solvent (1.8 mg **Phz** + 2.1 mg **H_2ca** + 1 mL CH_3CN in the vial) was applied (Fig. S9). This clearly demonstrates that the muddy suspension is contributed from cocrystals rather than individual component materials. After standing the muddy suspension for 2 h, precipitates appeared at the bottom of the vial, and only wires were obtained from drop-casting of the upper solution (Fig. 3c). However, if more solvent was used (1.8 mg **Phz** + 2.1 mg **H_2ca** + 7 mL CH_3CN in the vial), all the starting material was completely dissolved without forming precipitates, and only wires were acquired from drop-casting (Fig. 3d). Hence, the above observations allow us to infer that the precipitates are PHCs, and the solubility of the formed **Phz-H_2ca** complex in acetonitrile is significantly lowered than those of single-component materials, **Phz** or **H_2ca**. **Phz-H_2ca** can be regarded as a new dimolecular single species, rather than a simple mixture of **Phz** and **H_2ca** nor a so-called "molecular level heterojunction" [25].

Here we know that PHC wires can be selectively prepared from drop-casting of low-concentration solution, while plates are only formed under oversaturation. More interestingly, after standing the mixed solution (1.8 mg **Phz** + 2.1 mg **H_2ca** + 5 mL CH_3CN in the vial) for 3 d, wires disappeared and more plates were found on the substrate (Fig. S10a, b) from drop-casting of muddy suspension (not the upper solution). The corresponding XRD profiles of the obtained crystals on the substrate (Fig. S10c) with significantly lowered (10−1) and (20−2) diffraction peaks further confirm that the plates are dominated with almost no wires, consistent with the captured optical images. It thereby indicates that the plate is a more thermodynamically stable morphology of PHC.

In order to understand the different self-assembly processes triggered by different applied experimental conditions, the growth and equilibrium morphology of PHC was simulated using the Materials Studio software (Accelrys Inc., USA) [39–42] (Fig. 3e, f). Based on the calculation results, the attachment energy [39] E_{att} (*hkl*) of cocrystal faces (*hkl*) follows the order: E_{att} (020) > E_{att} (200) > E_{att} (10−1) ≈ E_{att} (002) (Table 1), and the proposed formula [43]:

$$R^{rel}_{\{hkl\}} = A \times E^{att}_{\{hkl\}},$$

where R_{hkl} is the relative growth rate of face (*hkl*); *A* is a proportional constant, illustrates that the growth rate of crystal face is proportional to its E_{att} (E_{att} means the energy released when two layers of the crystal structure {*hkl*} are brought together). Thus the (020) face with the largest E_{att} can grow fast to form 1D wire along the [020] direction even under low precursor concentration in the experiment (*vide supra*), whereas the (002) and (10−1) faces with the smallest E_{att} finally become the largest faces, and thus can be detected by the XRD measurements (Fig. S6). In this regard, wire belongs to the growth morphology of PHC and is kinetically stable. In comparison, the calculated E_{surf} (*hkl*) of PHC follows the order: E_{surf} (10−1) > E_{surf} (200) = E_{surf} (020) > E_{surf} (002). Based on the following equation [39]:

$$R^{rel}_{\{hkl\}} \propto C \times \exp\left(-\Delta G^{\neq}_{\{hkl\}} / k_B T\right),$$

where ΔG is the activation free energy for the growth crystal face (*hkl*), *C* is the concentration of growth units (here is the **Phz-H_2ca** complex), k_B is the Boltzmann constant, and *T* is the Kelvin temperature, and the relative growth rate of face (*hkl*) R_{hkl} depends on the kinetic growth barrier ΔG. Because the growth barrier of crystal face is inversely proportional to its E_{surf}, the crystal faces with higher E_{surf} and lower growth barrier therefore can

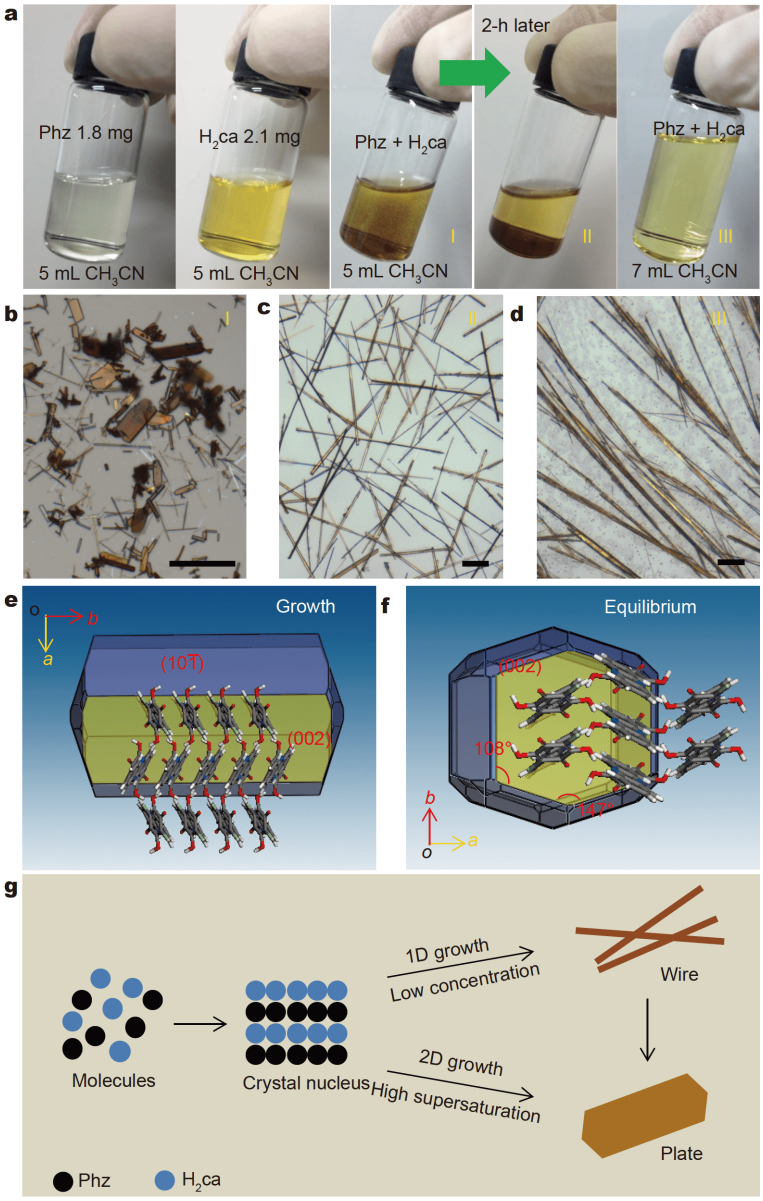

Figure 3 Cocrystal nucleation and growth. (a) Optical images of solutions prepared from different experimental conditions. Optical images of (b) the cocrystals obtained from drop-casting of the 5 mL solution immediately, (c) the wires obtained from the same 5 mL solution after standing for 2 h (the supernatant solution) and (d) the wires obtained from drop-casting of the 7 mL solution. All the scale bars are 50 μm. The simulated (e) growth and (f) equilibrium morphology of PHC from the Materials Studio Package. (g) The proposed nucleation and growth mechanism for PHCs.

grow faster [39]. Hence, the growth barrier of (200) and (020) faces smaller than that of (002) can be overcome under oversaturation in the experiments, while that of (002) face with the smallest E_{surf} (the largest growth barrier) still cannot. It therefore leads to the expansion along the [200] and [020] directions with a dominant (002) face, which is detected in the XRD experiment (Fig. S6). Moreover, the simulated equilibrium morphology with intersection angles of 147° and 108° (Fig. 3f) is in accord well with the experimental results (Fig. 1d, e). Thus, the 2D plate belongs to the equilibrium morphology of PHC and is thermodynamically stable.

A nucleation and growth mechanism for PHC is therefore proposed (Fig. 3g). In a typical crystal nucleation and growth process, **Phz** and **H_2ca** molecules start to recognize each other to form a new dimolecular species when the solvent is gradually evaporated, and self-assemble *via* π-π stacking, hydrogen-bonding, and van

Table 1 The calculated E_{att} and E_{surf} by using the Materials Studio Package [39]

Miller index	E_{surf} (Total) (kcal mol^{-1})	Total facet area	E_{att} (Total) (kcal mol^{-1})	Total facet area
(002)	0.16	30.1%	−31.31	36.3%
(110)	0.22	12.0%	−82.34	9.2%
(11−2)	0.23	10.5%	−84.36	0.6%
(200)	0.24	10.9%	−64.26	/
(10−1)	0.25	8.3%	−34.10	34.6%
(020)	0.24	/	−108.23	/

der Waals forces from "one to few", large aggregates to initial crystal nucleus and bulk crystals. If low precursor concentration was applied initially, the (020) face of co-crystal nucleus is predominately grown (1D self-assembly) under the driving force of π-π interactions; if the applied solution was highly oversaturated, the growth barrier of (200) and (020) faces is overcome, and the 2D self-assembly along these two directions under the driving forces of hydrogen bond and π-π interactions respectively is triggered immediately, leading to hexagon plate morphology. Therefore, the formation mechanism and different self-assembly manners of PHCs are fully understood and clearly exhibited, providing a standard reference for further controlling the polymorph of organic cocrystals.

Raman spectroscopy and anisotropy

The vibrational characteristics of PHC wires and plates were fully investigated. In a typical experiment, micro-area Raman spectra of crystals were obtained on an inVia-Reflex Raman spectrometer (Renishaw, UK) with the λ = 785 nm laser excitation (Fig. 4a). Raman signals were collected from the *in-situ* position where the laser beam was focused on. The glass substrate with samples was on a commercially purchased rotary table for the anisotropic investigations. The Raman spectra (Fig. 4b) with sharp strong peaks collected from individual crystals illustrate that they are highly single crystalline in nature, consistent with the TEM and SAED results (*vide supra*), and both of the wires and plates show the same result but different from those of **Phz** and **H_2ca** crystals. It clearly demonstrates that the wires and plates are indeed a composite of **Phz** and **H_2ca** materials, and the intermolecular interactions are significantly changed after co-crystallization. More specifically, the 732 cm^{-1} Raman band of **Phz** (assigned to CCC planar deformation, *v*9) [44,45] is shifted to 745 cm^{-1}, and the 1010 cm^{-1} band (CH bend, *v*8) is changed to 1016 cm^{-1}, while the 1403 cm^{-1} (ν_{c-c} phen ring) and 1417 cm^{-1} (combination band) bands are shifted to 1410 cm^{-1} in PHCs. And the 542 cm^{-1} Raman band of **H_2ca** (C–C_{str}, C=C_{str}, asym. Def.) [46] is changed to 529 cm^{-1}, while the 1653 cm^{-1} (C=C_{str}) band is shifted to 1635 cm^{-1} after co-crystallization. All the above spectroscopic shifts imply the formation of strong hydrogen bond in the cocrystals [16], which is similarly reflected by the changes in the Fourier transform infrared (FTIR) spectra (Fig. S16).

Furthermore, anisotropic Raman spectra of individual PHC wire and plate were studied in order to investigate the photon-lattice interactions and gain a deeper understanding of the structure information and structure-property relationship [47]. The Raman spectroscopic technique is known as a powerful tool to study the phonon symmetries [48], atomic displacement [48], lattice dynamics [49] and intermolecular transfer integrals (responsible for the charge mobility and can be modulated by Peierls electron-phonon coupling) [50]. In a typical experiment, a λ = 785 nm excitation semiconductor

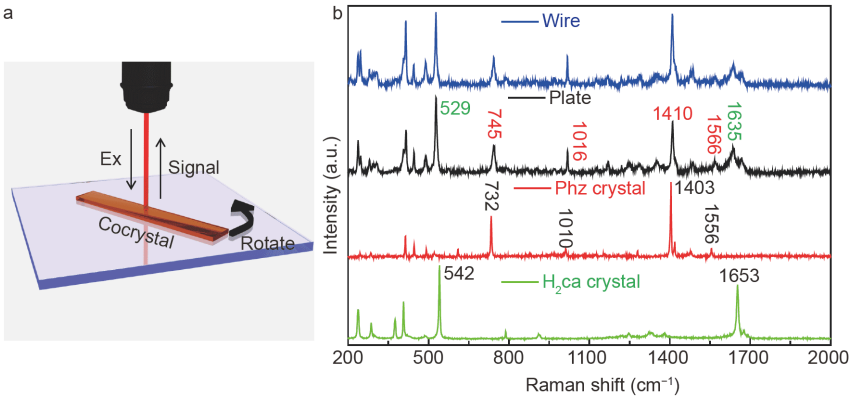

Figure 4 Raman spectroscopy. (a) Schematic diagram of the Raman spectrometer in the experiments. (b) The collected Raman spectra of individual crystals on the glass substrate (λ_{ex} = 785 nm).

laser was used and the glass substrate with PHCs on it was rotated (Fig. 5b, substrate rotation angle θ = 0°). The Raman spectra recorded from individual PHC wire is largely varied when θ is changed (Fig. 5a), and the relationship between the intensity of Raman signal and θ is displayed (Fig. 5c–f). The 528 cm^{-1} band (C–C_{str}, C=C_{str}, asymmetric deformation of **H_2ca** molecules in the wire) gives a maximum when the polarization of excitation laser is almost parallel to the growth direction ([010]) (Fig. 5c, θ = 90°), while the 743 cm^{-1} Raman signal (CCC planar deformation of **Phz** molecules in the wire) reaches a maximum when the laser polarization is nearly perpendicular to the elongated axis ([010] direction) (Fig. 5d, θ = 170°). Moreover, the corresponding anisotropic ratio (maximum/minimum) of 528 cm^{-1} band (r_{528}) is 2.13, while that of 743 cm^{-1} band (r_{743}) is calculated to be 1.81. These clearly illustrate the different symmetries [48,49] of two Raman-active vibrational modes in the wire, and the 1409 cm^{-1} (θ = 170°, Fig. 5f) and 416 cm^{-1} (θ = 0°, Fig. 5e) modes show the similar results as that of 743 cm^{-1} band. Notably, the variation of these Raman bands may also be related to the atomic displacements in the wire (proton-displacive and oxygen atom motion), as noted previously [16,47,48].

In comparison, individual PHC plate exhibits different anisotropic Raman spectra (Fig. 6a). The polarization of 528 cm^{-1} Raman-active vibrational mode in the plate is nearly parallel to its [100] direction (Fig. 6c, θ = 20°), whereas the 743 cm^{-1} band is changed to a maximum when the elongated axis ([010] direction) of the plate is almost perpendicular to the laser polarization (Fig. 6d, θ = 10°), and polarizations of the 416 cm^{-1} (Fig. 6e, θ = 100°) and 1409 cm^{-1} bands (Fig. 6f, θ = 170°) are also exhibited. The corresponding anisotropic ratio r_{528} is measured to be 1.68, and r_{743} is 5.53, different from those of PHC wires. Similarly, different Raman bands show different polarizations, and it is attributed to the different symmetries of Raman modes and the atomic displacements in the plate. More interestingly, the same Raman bands of PHC wire and plate show different polarizations (Fig. 5c *vs.* Fig. 6c, Fig. 5e *vs.* Fig. 6e, and Table 2), which is intrinsically due to their distinct molecular packings/orientations, consistent with the TEM, SAED, and XRD results (*vide supra*), though they belong to the same co-crystal phase. Importantly, ferroelectric cocrystal material is one of promising systems for advanced electronic devices and applications [17], so we performed piezo-response force microscopy (PFM) measurement. Surprisingly, as a typical displacive-type ferroelectric material (Curie temperature T_c = 253 K) [16,36], the two

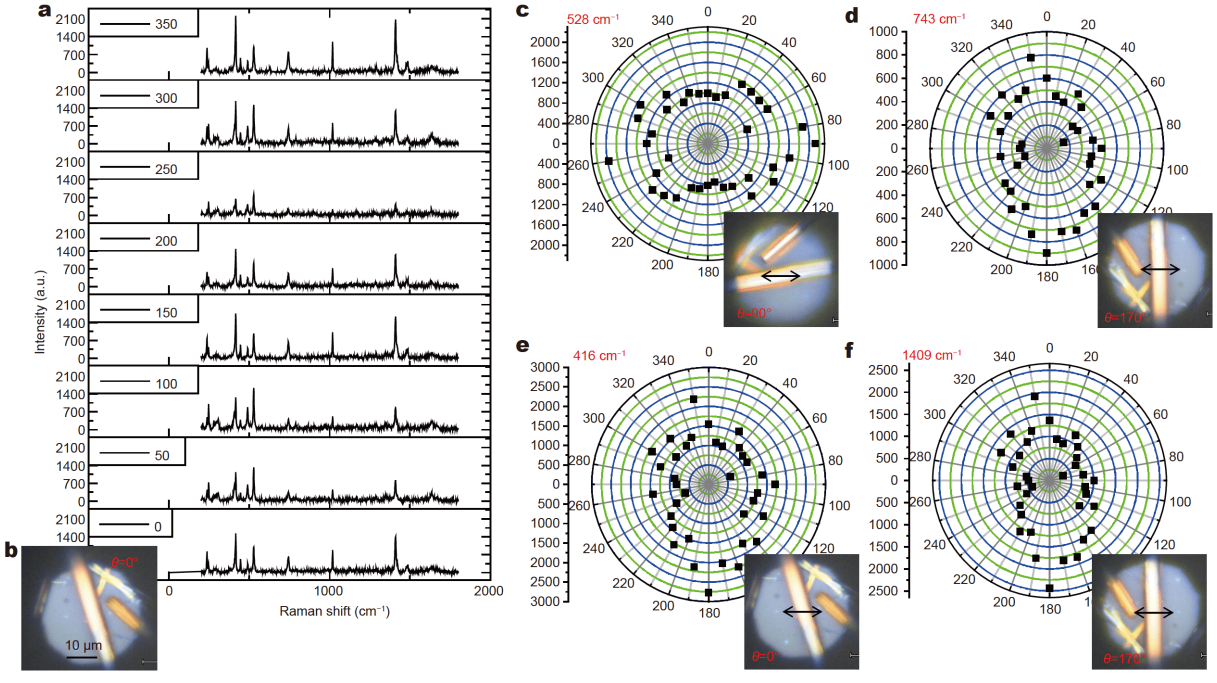

Figure 5 Anisotropic Raman spectra of PHC wire. (a) The Raman spectra of individual wire. (b) The corresponding optical image of individual wire on the glass substrate (the substrate rotation angle θ = 0°). The polarization of excitation 785 nm laser is also shown. The collected intensities of (c) 528 cm^{-1}, (d) 743 cm^{-1}, (e) 416 cm^{-1} and (f) 1409 cm^{-1} Raman peaks are changed as the substrate rotates. Inserts are the corresponding optical images of PHC on the glass substrate when the Raman signal gives a maximum.

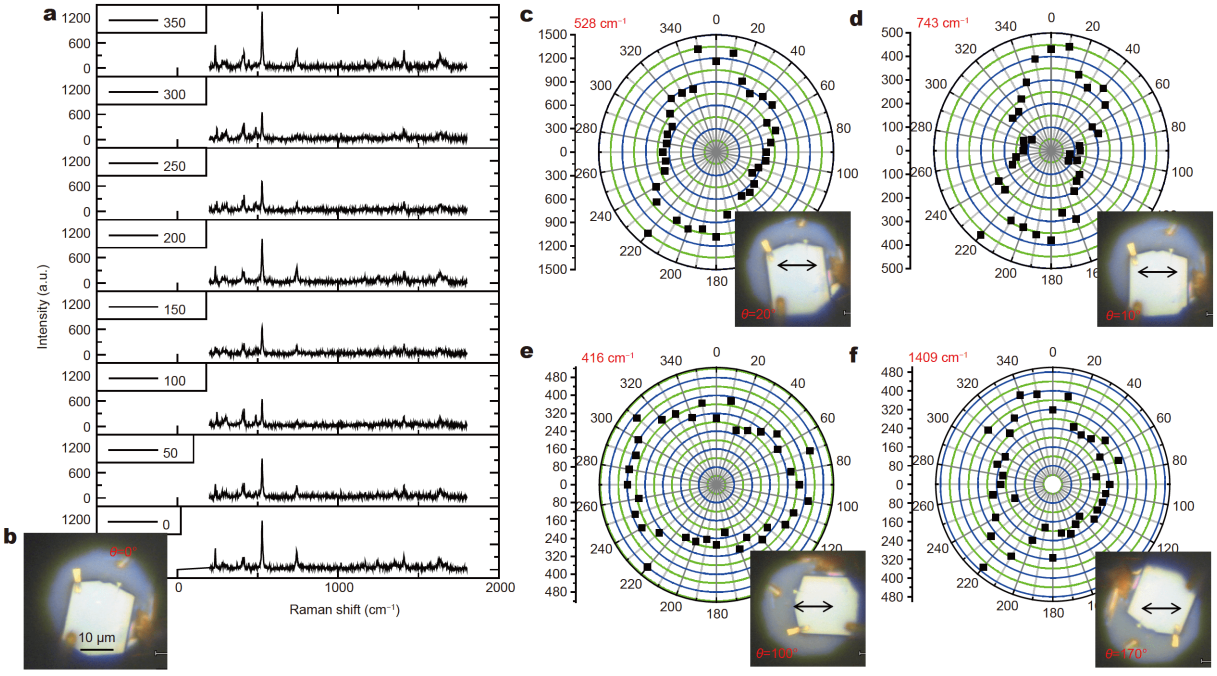

Figure 6 Anisotropic Raman spectra of PHC plate. (a) The Raman spectra of individual plate. (b) The corresponding optical image of individual plate on the glass substrate (the substrate rotation angle θ = 0°). The polarization of excitation 785 nm laser is also shown. The collected intensities of (c) 528 cm^{-1}, (d) 743 cm^{-1}, (e) 416 cm^{-1}, and (f) 1409 cm^{-1} Raman peaks are changed as the substrate rotates. Inserts are the corresponding optical images of PHC on the glass substrate when the Raman signal gives a maximum.

types of PHCs show different mag-voltage and phase-voltage curves (Fig. S17) at room temperature under ambient conditions, again corresponding to their different molecular packings/orientations [51].

CONCLUSIONS

As a final remark, a new wire-like morphology of PHC has been firstly demonstrated and fully confirmed by AFM, TEM, XRD, crystal color, UV-Vis absorption spectra, DSC, and solid-state ^{1}H NMR measurements. The structure characterizations indicate that the new obtained PHC wires are grown along the [010] direction, which is different from the 2D hexagon plates expanding along the [010] and [100] directions. By tuning the applied experimental conditions, we find that low **Phz-H$_2$ca** precursor concentration is beneficial for 1D self-assembly along the [010] direction under the driving force of π-π interactions to form kinetic stable wires, while only supersaturation starts the 2D self-assembly along [100] and [010] directions under the driving forces of hydrogen bond and π-π interactions respectively to generate thermodynamically stable plates. The Materials Studio software simulations attribute these experimental observations to the largest E_{att} of (020) face and the smallest E_{surf} of (002) face. The self-assembly and growth kinetics of PHCs are therefore rationally controlled and a reasonable nucleation and growth mechanism is proposed, thus providing a standard reference for further controlling polymorph of organic cocrystals. The vibrational characteristics of two types of PHCs are investigated by Raman and FTIR spectra, both of which clearly demonstrate the formation of strong hydrogen bond. And different Raman-active vibrational modes of the wire (or plate) exhibit distinct anisotropic response, which is due to the different symmetries of Raman modes and the atomic displacements in PHCs. Moreover, the same Raman bands of PHC wire and PHC plate display different polarizations, which is intrinsically due to their distinct molecular packings/orientations as shown in the

Table 2 The anisotropic Raman response of PHC wire and PHC plate

Raman signal	PHC wire		PHC plate	
	Direction	r	Direction	r
528 cm^{-1}	∥[010]	2.13	∥[100]	1.68
743 cm^{-1}	⊥[010]	1.81	∥[100]	5.53
1409 cm^{-1}	⊥[010]	/	∥[100]	/
416 cm^{-1}	⊥[010]	/	∥[010]	/

TEM and XRD experiments. The work helps to rationally prepare cocrystal materials with desired functions, and gain a deeper understanding of their intrinsic physicochemical properties. Further related research, underway in our laboratory, are focusing on the polymorph and formation mechanism of molecular cocrystals, developing temperature-dependent and ultrafast time-resolved Raman spectroscopy to reveal their structural information, as well as achieving high T_c organic ferroelectrics.

Received 3 April 2020; accepted 25 April 2020; published online 22 July 2020

1 Liu J, Zhang H, Dong H, *et al.* High mobility emissive organic semiconductor. Nat Commun, 2015, 6: 10032
2 Zhu M, Pan S, Wang Y, *et al.* Unravelling the correlation between charge mobility and cocrystallization in rod-rod block copolymers for high-performance field-effect transistors. Angew Chem Int Ed, 2018, 57: 8644–8648
3 Dou L, Zheng Y, Shen X, *et al.* Single-crystal linear polymers through visible light-triggered topochemical quantitative polymerization. Science, 2014, 343: 272–277
4 Li R, Hu W, Liu Y, *et al.* Micro- and nanocrystals of organic semiconductors. Acc Chem Res, 2010, 43: 529–540
5 Wang C, Dong H, Jiang L, *et al.* Organic semiconductor crystals. Chem Soc Rev, 2018, 47: 422–500
6 Zhang C, Yan Y, Zhao YS, *et al.* From molecular design and materials construction to organic nanophotonic devices. Acc Chem Res, 2014, 47: 3448–3458
7 Qin Z, Gao H, Liu J, *et al.* High-efficiency single-component organic light-emitting transistors. Adv Mater, 2019, 31: 1903175
8 Guo L, Gu X, Zhu X, *et al.* Recent advances in molecular spintronics: Multifunctional spintronic devices. Adv Mater, 2019, 31: 1805355
9 Ding S, Tian Y, Li Y, *et al.* Organic single-crystal spintronics: Magnetoresistance devices with high magnetic-field sensitivity. ACS Nano, 2019, 13: 9491–9497
10 Zhu W, Yi Y, Zhen Y, *et al.* Precisely tailoring the stoichiometric stacking of perylene-TCNQ co-crystals towards different nano and microstructures with varied optoelectronic performances. Small, 2015, 11: 2150–2156
11 Zhang H, Jiang L, Zhen Y, *et al.* Organic cocrystal photovoltaic behavior: A model system to study charge recombination of C_{60} and C_{70} at the molecular level. Adv Electron Mater, 2016, 2: 1500423
12 Aitipamula S, Banerjee R, Bansal AK, *et al.* Polymorphs, salts, and cocrystals: What's in a name? Cryst Growth Des, 2012, 12: 2147–2152
13 Zhu W, Zhen Y, Dong H, et al. Organic cocrystal optoelectronic materials and devices. Prog Chem, 2014, 26: 1292–1306
14 Zhu W, Zheng R, Zhen Y, *et al.* Rational design of charge-transfer interactions in halogen-bonded co-crystals toward versatile solid-state optoelectronics. J Am Chem Soc, 2015, 137: 11038–11046
15 Zhang J, Tan J, Ma Z, *et al.* Fullerene/sulfur-bridged annulene cocrystals: Two-dimensional segregated heterojunctions with ambipolar transport properties and photoresponsivity. J Am Chem Soc, 2013, 135: 558–561
16 Horiuchi S, Ishii F, Kumai R, *et al.* Ferroelectricity near room temperature in co-crystals of nonpolar organic molecules. Nat Mater, 2005, 4: 163–166
17 Tayi AS, Kaeser A, Matsumoto M, *et al.* Supramolecular ferroelectrics. Nat Chem, 2015, 7: 281–294
18 Bolton O, Lee K, Kim HJ, *et al.* Activating efficient phosphorescence from purely organic materials by crystal design. Nat Chem, 2011, 3: 205–210
19 Bosshard C, Wong MS, Pan F, *et al.* Self-assembly of an acentric co-crystal of a highly hyperpolarizable merocyanine dye with optimized alignment for nonlinear optics. Adv Mater, 1997, 9: 554–557
20 Rao SM, Batra AK, Lal RB, *et al.* Mixed methyl-(2,4-dinitrophenyl)-aminopropanoate: 2-Methyl-4-nitroaniline crystal—A new nonlinear optical material. J Appl Phys, 1991, 70: 6674–6678
21 Zhu W, Dong H, Zhen Y, *et al.* Challenges of organic "cocrystals". Sci China Mater, 2015, 58: 854–859
22 Wuest JD. Co-crystals give light a tune-up. Nat Chem, 2012, 4: 74–75
23 Aakeröy C. Is there any point in making co-crystals? Acta Crystlogr B Struct Sci Cryst Eng Mater, 2015, 71: 387–391
24 Li R, Zhang X, Dong H, *et al.* Gibbs-curie-wulff theorem in organic materials: A case study on the relationship between surface energy and crystal growth. Adv Mater, 2016, 28: 1697–1702
25 Zhang J, Geng H, Virk TS, *et al.* Sulfur-bridged annulene-TCNQ co-crystal: A self-assembled "molecular level heterojunction" with air stable ambipolar charge transport behavior. Adv Mater, 2012, 24: 2603–2607
26 Briseno AL, Mannsfeld SCB, Ling MM, *et al.* Patterning organic single-crystal transistor arrays. Nature, 2006, 444: 913–917
27 Zhang C, Zou CL, Zhao Y, *et al.* Organic printed photonics: From microring lasers to integrated circuits. Sci Adv, 2015, 1: e1500257
28 Bernstein J, Davey RJ, Henck JO. Concomitant polymorphs. Angew Chem Int Ed, 1999, 38: 3440–3461
29 Hu P, Ma L, Tan KJ, *et al.* Solvent-dependent stoichiometry in perylene-7,7,8,8-tetracyanoquinodimethane charge transfer compound single crystals. Cryst Growth Des, 2014, 14: 6376–6382
30 Sun H, Wang M, Wei X, *et al.* Understanding charge-transfer interaction mode in cocrystals and solvates of 1-phenyl-3-(pyren-1-yl) prop-2-en-1-one and TCNQ. Cryst Growth Des, 2015, 15: 4032–4038
31 Bechgaard K, Kistenmacher TJ, Bloch AN, *et al.* The crystal and molecular structure of an organic conductor from 4,4′,5,5′-tetramethyl-$\Delta^{2,2'}$-bis-1,3-diselenole and 7,7,8,8-tetracyano-*p*-quinodimethane [TMTSF-TCNQ]. Acta Crystlogr B Struct Sci, 1977, 33: 417–422
32 Pope M. Electronic Processes in Organic Crystals and Polymers. 2nd Ed. Oxford: Oxford University Press, 1999
33 Liu G, Liu J, Liu Y, *et al.* Oriented single-crystal-to-single-crystal phase transition with dramatic changes in the dimensions of crystals. J Am Chem Soc, 2014, 136: 590–593
34 Boterashvili M, Lahav M, Shankar S, *et al.* On-surface solvent-free crystal-to-co-crystal conversion by non-covalent interactions. J Am Chem Soc, 2014, 136: 11926–11929
35 Horiuchi S, Kumai R, Tokura Y. Room-temperature ferroelectricity and gigantic dielectric susceptibility on a supramolecular architecture of phenazine and deuterated chloranilic acid. J Am Chem Soc, 2005, 127: 5010–5011
36 Amano M, Yamamura Y, Sumita M, *et al.* Calorimetric and dielectric study of organic ferroelectrics, phenazine-chloranilic acid, and its bromo analog. J Chem Phys, 2009, 130: 034503

37 Andersen EK. The crystal and molecular structure of hydroxyquinones and salts of hydroxyquinones. V. Hydronium nitranilate, nitranilic acid hexahydrate. Acta Cryst, 1967, 22: 204–208
38 Lee T, Chen HR, Lin HY, *et al.* Continuous co-crystallization as a separation technology: The study of 1:2 co-crystals of phenazine-vanillin. Cryst Growth Des, 2012, 12: 5897–5907
39 Kang L, Fu H, Cao X, *et al.* Controlled morphogenesis of organic polyhedral nanocrystals from cubes, cubooctahedrons, to octahedrons by manipulating the growth kinetics. J Am Chem Soc, 2011, 133: 1895–1901
40 Winn D, Doherty MF. Modeling crystal shapes of organic materials grown from solution. AIChE J, 2000, 46: 1348–1367
41 Piaggi PM, Parrinello M. Predicting polymorphism in molecular crystals using orientational entropy. Proc Natl Acad Sci USA, 2018, 115: 10251–10256
42 Zhu W, Zhu L, Sun L, *et al.* Uncovering the intramolecular emission and tuning the nonlinear optical properties of organic materials by cocrystallization. Angew Chem Int Ed, 2016, 55: 14023–14027
43 Liu XY, Boek ES, Briels WJ, *et al.* Prediction of crystal growth morphology based on structural analysis of the solid-fluid interface. Nature, 1995, 374: 342–345
44 Durnick TJ, Wait Jr. SC. Vibrational spectra and assignments for phenazine. J Mol Spectr, 1972, 42: 211–226
45 Li WH, Li XY, Yu NT. Surface-enhanced hyper-Raman scattering and surface-enhanced Raman scattering studies of electroreduction of phenazine on silver electrode. Chem Phys Lett, 2000, 327: 153–161
46 Pawlukojc A, Bator G, Sobczyk L, *et al.* Inelastic neutron scattering, Raman, infrared and DFT theoretical studies on chloranilic acid. J Phys Org Chem, 2003, 16: 709–714
47 Fujioka J, Horiuchi S, Kida N, *et al.* Anisotropic polarization π-molecular skeleton coupled dynamics in proton-displacive organic ferroelectrics. Phys Rev B, 2009, 80: 125134
48 Kim H, Ko H, Kim SM, *et al.* Polarization-dependent anisotropic Raman response of CVD-grown vertically stacked MoS_2 layers. J Raman Spectrosc, 2020, 51: 774–780
49 Venuti E, Bilotti I, Della Valle RG, *et al.* Polarized Raman spectra of a rubrene single crystal. J Phys Chem C, 2008, 112: 17416–17422
50 Troisi A. Prediction of the absolute charge mobility of molecular semiconductors: The case of rubrene. Adv Mater, 2007, 19: 2000–2004
51 Fu DW, Cai HL, Liu Y, *et al.* Diisopropylammonium bromide is a high-temperature molecular ferroelectric crystal. Science, 2013, 339: 425–428

Acknowledgements This work was supported by the National Natural Science Foundation of China (51303185, 21021091, 51033006, 51222306, 51003107, 61201105, 3591027043, 91222203, 91233205, 21473222 and 21773040), the Ministry of Science and Technology of China (2011CB808400, 2011CB932300, 2013CB933403, 2013CB933500 and 2014CB643600), and the Chinese Academy of Sciences (Y42D0A12D1 and Y42D0412D1).

Author contributions Hu W directed the project; Wang Y and Huang C performed the PFM experiments; Zhu W performed the other experiments and Materials Studio software simulations; Zhu L performed the DFT computations; Zhen Y, Dong H, Wei Z and Guo D contributed to the general discussion. All the authors contributed to the manuscript and supporting information writing.

Conflict of interest The authors declare that they have no conflict of interest.

Supplementary information Experimental details and supporting data are available in the online version of the paper.

Weigang Zhu obtained his BE degree from the University of Electronic Science and Technology of China (UESTC) (2011) and PhD degree from the Institute of Chemistry, Chinese Academy of Sciences (ICCAS) under the supervision of Professor Wenping Hu (2016). He then carried out postdoctoral research training in Professor Tobin J. Marks's group at Northwestern University (2019). His research interests include one-dimensional hybrid nanomaterials, molecular co-crystals, and organic photovoltaics.

Wenping Hu is currently a professor at the Department of Chemistry, Tianjin University, and the Founder & Director of Tianjin Key Laboratory of Molecular Optoelectronic Sciences. He obtained his PhD degree from ICCAS in 1999. He then joined Osaka University as a research fellow of Japan Society for the Promotion of Sciences, and Stuttgart University as an Alexander von Humboldt fellow. In 2003, he worked for Nippon Telephone and Telegraph, and then returned to ICCAS and was promoted as full professor. His research focuses on molecular electronics.

Phz-H_2ca铁电共晶的形貌控制及其各向异性拉曼光谱

朱伟钢[1,2], 王云丽[3], 黄程程[4], 朱凌云[5], 甄永刚[1], 董焕丽[1], 魏志祥[5], 郭栋[3,4], 胡文平[1,6*]

摘要 本文首次报道了**Phz-H_2ca**铁电共晶的一种线状形貌, 并通过原子力显微镜、透射电子显微镜、X射线衍射、紫外可见吸收光谱、差示扫描量热法和固体核磁等实验手段证实. 共晶成核生长实验和Materials Studio软件模拟研究发现, (020)面具有最大的结合能, 在较低前驱体浓度下晶核沿[010]方向组装形成动力学稳定的线状形貌, (002)面具有最小的表面能和最大生长势垒, 即使在超饱和前驱体浓度下也只有(200)和(020)等晶面的生长势垒被突破, 使晶核沿[100]和[010]两个方向生长为热力学稳定的六边形片状形貌. 微区拉曼光谱实验研究表明, 两种**Phz-H_2ca**共晶的拉曼峰具有截然不同的各向异性响应性, 归因于其不同的分子排布取向. 该研究工作实现了对分子共晶的控制制备, 阐明了其中的结构功能关系, 为共晶功能材料的进一步大规模应用提供了有力借鉴.

